



Research paper

Kinetic, thermodynamic and structural analysis of tamiphosphor binding to neuraminidase of H1N1 (2009) pandemic influenza



Carlos Berenguer Albiñana^a, Aleš Machara^a, Pavlína Řezáčová^{b,c}, Petr Pachtl^b, Jan Konvalinka^{b,d,**}, Milan Kožíšek^{b,*}

^a Department of Organic Chemistry, Faculty of Science, Charles University, Hlavova 8, 128 00, Prague 2, Czech Republic

^b Institute of Organic Chemistry and Biochemistry, Academy of Sciences of the Czech Republic, Gilead Sciences and IOCB Research Center, Flemingovo n. 2, 166 10, Prague 6, Czech Republic

^c Institute of Molecular Genetics, Academy of Sciences of the Czech Republic, Vídeňská 1083, 140 00, Prague 4, Czech Republic

^d Department of Biochemistry, Faculty of Science, Charles University, Hlavova 8, 128 00, Prague 2, Czech Republic

ARTICLE INFO

Article history:

Received 19 January 2016

Received in revised form

11 April 2016

Accepted 3 May 2016

Available online 7 May 2016

Keywords:

Influenza neuraminidase

Osetamivir

Tamiphosphor

Isothermal titration calorimetry

Crystal structure

Lattice-translocation defect

ABSTRACT

Influenza virus causes severe respiratory infections that are responsible for up to half a million deaths worldwide each year. Two inhibitors targeting viral neuraminidase have been approved to date (oseltamivir, zanamivir). However, the rapid development of antiviral drug resistance and the efficient transmission of resistant viruses among humans represent serious threats to public health.

The approved influenza neuraminidase inhibitors have (oxa)cyclohexene scaffolds designed to mimic the oxonium transition state during enzymatic cleavage of sialic acid. Their active forms contain a carboxylate that interacts with three arginine residues in the enzyme active site. Recently, the phosphonate group was successfully used as an isostere of the carboxylate in oseltamivir, and the resulting compound, tamiphosphor, was identified as a highly active neuraminidase inhibitor. However, the structure of the complex of this promising inhibitor with neuraminidase has not yet been reported.

Here, we analyzed the interaction of a set of oseltamivir and tamiphosphor derivatives with neuraminidase from the A/California/07/2009 (H1N1) influenza virus. We thermodynamically characterized the binding of oseltamivir carboxylate or tamiphosphor to the neuraminidase catalytic domain by protein microcalorimetry, and we determined crystal structure of the catalytic domain in complex with tamiphosphor at 1.8 Å resolution. This structural information should aid rational design of the next generation of neuraminidase inhibitors.

© 2016 Elsevier Masson SAS. All rights reserved.

1. Introduction

Influenza virus causes respiratory infections in birds and mammals, and during seasonal epidemics, influenza can spread easily from person to person. Several human influenza pandemics

Abbreviations: 4-MUNANA, 2'-(4-methylumbelliferyl)- α -D-N-acetylneuraminic acid; NA, neuraminidase; PDB, protein data bank; ITC, isothermal titration calorimetry.

* Corresponding author. Institute of Organic Chemistry and Biochemistry, Academy of Sciences of the Czech Republic, Gilead Sciences and IOCB Research Center, Flemingovo n. 2, 166 10, Prague 6, Czech Republic.

** Corresponding author. Institute of Organic Chemistry and Biochemistry, Academy of Sciences of the Czech Republic, Gilead Sciences and IOCB Research Center, Flemingovo n. 2, 166 10, Prague 6, Czech Republic.

E-mail addresses: konval@uochb.cas.cz (J. Konvalinka), milan.kozisek@uochb.cas.cz (M. Kožíšek).

have occurred in the last century, each caused by a new strain of the virus. The most severe pandemic began in 1918 (the “Spanish flu,” caused by an H1N1 virus) and resulted in over 50 million deaths worldwide during a two-year period. Other severe pandemics appeared in Asia in 1957 (“Asian flu,” H2N2) and 1968 (“Hong Kong flu,” H3N2) [1,2]. The most recent pandemic strain, identified in 2009, had a swine origin (“swine flu,” H1N1) [3]. Furthermore, a new variant of an extremely virulent H7N9 avian virus was detected in China in 2013 [4]. Two types of antivirals are clinically available to target different steps in the influenza viral cycle. The antiviral drug amantadine blocks a viral ion channel formed by the M2 protein, preventing the virus from infecting host cells. However, the United States Centers for Disease Control and Prevention (CDC) recommends avoiding use of M2 inhibitors due to the high level of drug resistance development. The second type of available drugs approved by the Food and Drug Administration (FDA) is the class of

neuraminidase inhibitors. The influenza glycoprotein neuraminidase (NA) is an essential enzyme for the last step of the viral cycle – the release of viral particles from the host cell. Neuraminidase cleaves sialic acid linked to the host cell receptor, facilitating viral shedding. Without this process, the viral particle is not released from the plasma membrane, and the infection does not spread [5]. To date, two antiviral drugs targeting NA have been approved by the FDA for treatment of influenza – oseltamivir (Tamiflu; Hoffmann-La Roche) and zanamivir (Relenza; GlaxoSmithKline). While oseltamivir has good oral bioavailability, zanamivir must be delivered directly to the respiratory tract through an inhaler. Two other neuraminidase inhibitors, peramivir (BioCryst Pharmaceuticals) and laninamivir (Biota Pharmaceuticals), are currently in clinical evaluation and are approved in various countries for emergency treatment during influenza pandemics [6,7].

The recent emergence of new pandemic influenza strains and the increasing resistance against approved NA inhibitors have emphasized the need for development of new, effective anti-influenza drugs active against resistant viral strains and different NA subtypes. Traditional structure-based drug design is based on the lock-and-key hypothesis and assumes a static protein binding site. The inhibitors developed by this strategy are conformationally constrained and pre-shaped to the selected enzyme target, and thus unable to accommodate changes caused by viral mutations. High-affinity adaptive inhibitors can be designed by thermodynamic optimization, as described in detail by Ohtaka and Freire [8], and isothermal titration calorimetry (ITC) has become an essential tool in molecular design. The binding affinity is determined by the Gibbs free energy, which is a function of enthalpic and entropic contributions. Analysis of these two contributions is essential for development of optimized inhibitors with better adaptability and selectivity. Briefly, the enthalpic contribution reflects direct strong interactions between the ligand and the protein (hydrogen bonds and van der Waals interactions) relative to those with the solvent. On the other hand, the entropic contribution largely reflects hydration effects and conformational changes. This biochemical characterization could bring deeper insight into the further development of adaptive NA inhibitors that may be useful during future influenza pandemics. Interestingly, no thermodynamic analysis of complex formation between NA and an FDA-approved inhibitor has been published to date. The only report about the thermodynamics of an inhibitor binding to NA describes the calorimetric analysis of the weak binding of substrate derivatives (3' and 6'-sialyllactosamines) to N2 NA [9].

Recently, the introduction of a phosphonate group as an isostere of the carboxylate in oseltamivir was described, and the resulting derivative was named tamiphosphor. The acidic moiety was previously identified as essential for direct binding of the inhibitor in the active site pocket, where it forms strong interactions with three arginine residues [10]. The tamiphosphor binding mode has been proposed based on molecular modeling in which the phosphonate compound was docked using the crystal structure of oseltamivir carboxylate with N1 avian NA A/Vietnam/1203/04 [11]. Compared with NA complexed with oseltamivir carboxylate, in which 6 pairs of hydrogen bonds were formed in the active site with the arginine triad, the tamiphosphor binding model proposes extensive hydrogen bonding interactions, with 8 pairs of hydrogen bonds [12]. Because the high polarity of the phosphonate group in tamiphosphor might compromise its bioavailability, different formulations and new ester prodrugs were studied [10,13].

We set out to analyze the structure and thermodynamics of tamiphosphor binding to NA from the pandemic A/California/07/2009(H1N1) influenza virus (NA2009_{wt}). Biochemical characterization of the promising NA inhibitor tamiphosphor promises to aid rational design of more potent NA inhibitors active against resistant

strains.

2. Results and discussion

2.1. Synthesis of neuraminidase inhibitors

The compounds presented here were prepared as outlined in Schemes 1 and 2. Briefly, oseltamivir carboxylate (**1**) and its guanidine-containing congener (**2**) were prepared from commercially available oseltamivir phosphate (**3**). Simple hydrolysis, pH adjustment and purification yielded compound **1**. Congener **2** was prepared in a similar fashion. The only additional steps were installation of the guanidium moiety with Boc-protected thiourea and subsequent Boc deprotection with TFA.

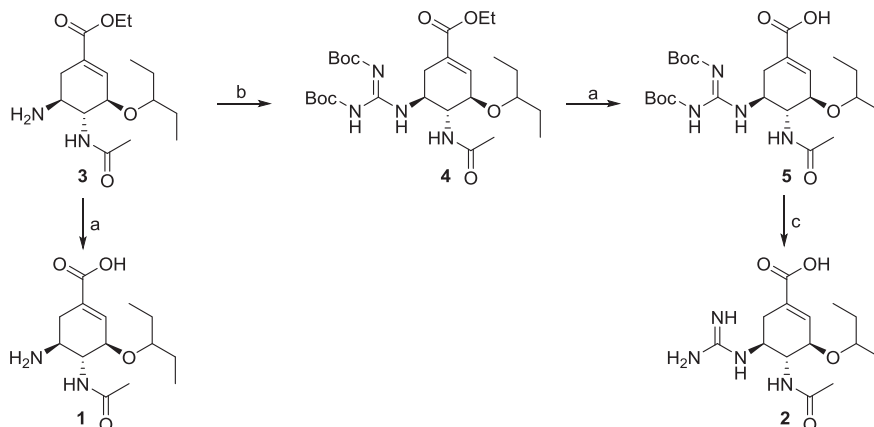
The synthetic strategy used for preparation of tamiphosphor (**6**) and its derivatives involved preparation of an appropriately substituted 1-bromocyclohexene (**9**), which was obtained by a modified procedure reported by Gunasekera [14]. Acid **8** was converted into a Barton thioester (not isolated) in a one-pot reaction by the action of HOTT (*N,N,N',N'*-tetramethyl-5-(1-oxido-2-pyridyl)thiuronium hexafluorophosphate). Upon irradiation in the presence of bromotrichloromethane, this afforded bromide **9**. Then, palladium-catalyzed phosphorylation with dimethyl phosphite gave the desired phosphonate **10** in fair yield. With the parent compound in hand, we employed different synthetic strategies to prepare the desired compounds. One strategy involved Boc deprotection followed by the mercury-catalyzed installation of the guanidium moiety. Treatment of intermediate **11** with bromotrimethylsilane resulted in ester hydrolysis and full deprotection of the guanidium moiety, yielding derivative **12**. The key intermediate was also subjected to selective mono-O-demethylation with sodium hydroxide to provide **13**, which either yielded **14** upon Boc deprotection or was directly converted to **6** by treatment with bromotrimethylsilane. All prepared compounds were purified by preparative HPLC; collected fractions were lyophilized and used as obtained.

2.2. Kinetic analysis of inhibitor binding to pandemic neuraminidase

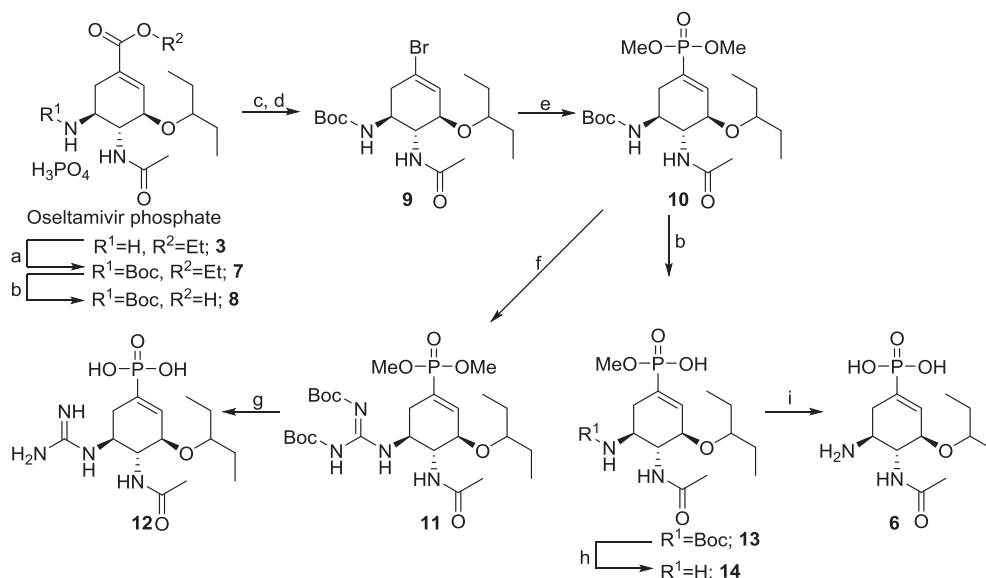
The activity of NA2009_{wt} in the presence and absence of inhibitors was analyzed using the fluorescent substrate 4-MUNANA, as previously described [15,16]. Results of these kinetic analyses are shown in Fig. 1. Oseltamivir carboxylate (**1**) and tamiphosphor (**6**) had similar affinities toward pandemic NA2009_{wt} (inhibition constants of 24 nM and 26 nM, respectively). The kinetic data revealed the importance of an acidic group in the position of carboxylate in oseltamivir carboxylate (compare compounds **3**, **6** and **14** with **1**). This finding is in agreement with structural analysis of oseltamivir binding to the active site of NA, showing strong electrostatic interactions between the carboxylate group and three arginine residues in NA [17]. The kinetic measurements also showed that substituting one phosphonic acid hydroxy group with a methoxy group (**14**) had a minimal effect on inhibition, while blocking the carboxylate (**3**) led to significant decrease in inhibitor effectiveness. Replacing the amino group with guanidine in oseltamivir carboxylate (**2**) or tamiphosphor (**12**) did not significantly affect inhibitor potency.

2.3. Isothermal titration calorimetry

The thermodynamics of binding of oseltamivir carboxylate (**1**) and tamiphosphor (**6**) to NA2009_{wt} were characterized by ITC. Both inhibitors bind to NA with large favorable enthalpic contributions (-10.8 ± 0.1 kcal/mol and -11.0 ± 0.1 kcal/mol, respectively) and



Scheme 1. Preparation of oseltamivir carboxylate and its analogues. Reagents and conditions: (a) 1. NaOH, 2. Amberlite (b) *N,N'*-di-(*tert*-butoxycarbonyl)thiourea, HgCl₂; (c) TFA/H₂O.



Scheme 2. Synthesis of tamiphosphor and its analogues. Reagents and conditions: (a) Boc₂O, Et₃N; (b) 1. NaOH, 2. Amberlite; (c) HOTT, Et₃N; (d) CBrCl₃; (e) (CH₃O)₂P(O)H, Et₃N, Pd(PPh₃)₄; (f) 1. TFA, 2. *N,N'*-di-Boc-1*H*-pyrazole-1-carboxamide, Et₃N; (g) (CH₃)₃SiBr, DCM; (h) TFA/H₂O; (i) 1. (CH₃)₃SiBr, 2,6-lutidine, 2. TFA/H₂O.

slightly unfavorable entropic contributions (1.5 ± 0.2 kcal/mol and 2.2 ± 0.2 kcal/mol, respectively) at the temperature of the experiments. The binding stoichiometries were close to 1, reflecting binding of one inhibitor molecule to each subunit of the NA2009_{wt} tetramer. Experiments performed in buffers with different enthalpies of ionization yielded the same binding enthalpies, indicating that under experimental conditions, there is no net proton transfer process coupled to inhibitor binding. All the thermodynamic results are summarized in Fig. 2.

As shown previously for HIV-1 protease, enthalpically driven inhibitors achieve high binding affinity, adaptability and selectivity and have superior drug resistance profiles [8]. A complete series of thermodynamic data have been determined for protease inhibitors that are used in the treatment of HIV-positive patients [18]. The binding of first-generation HIV-1 protease inhibitors was driven by a strong favorable entropy change, and these inhibitors were less effective against resistant viral variants [18,19]. Recently optimized second-generation inhibitors exhibit high adaptability to mutations associated with drug resistance. These inhibitors tend to have more favorable enthalpic contributions to the binding affinity, indicating

that the optimization resulted in more favorable interactions with HIV-1 protease and, importantly, made the compound less sensitive to mutations in the binding site of the target enzyme. Specifically, backbone-to-backbone hydrogen bonding was identified as a key interaction that led to favorable enthalpic contribution and rendered the inhibitor insensitive to amino acid mutations [18,20,21].

The favorable interaction enthalpy of NA inhibitors indicates that they form optimal direct interactions within the active site of the enzyme. This represents a promising characteristic for further rational design of next-generation NA inhibitors [22].

2.4. Crystal structure of pandemic neuraminidase in complex with tamiphosphor

The crystal structure of NA2009_{wt} in complex with tamiphosphor (6) was determined at 1.8 Å resolution. The crystal contained two protein molecules in the asymmetric unit; the tetrameric biological unit can be reconstructed from two symmetrically related dimers.

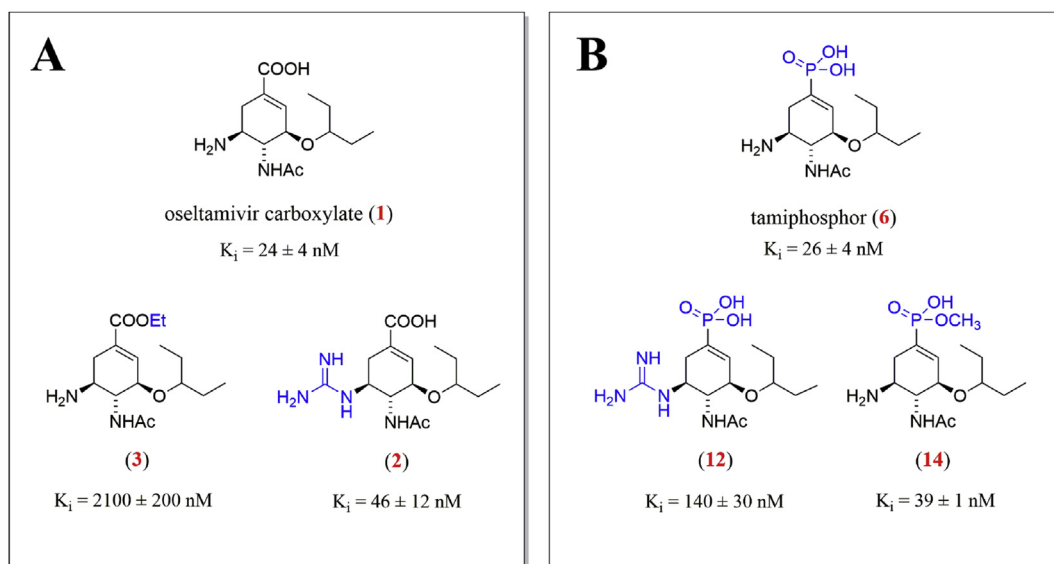


Fig. 1. Derivatives of oseltamivir carboxylate (A) and tamiphosphor (B). Substitutions for the carboxyl or amine group in oseltamivir are highlighted in blue. The inhibition constants (K_i values) were determined by fluorimetric assay using the substrate 4-MUNANA in 0.1 M MES, pH 6.15, 150 mM NaCl and 10 mM CaCl_2 at 37 °C. (For interpretation of the references to colour in this figure legend, the reader is referred to the web version of this article.)

The crystal contained a lattice-translocation defect. The lattice translocation vector was $(1/2, 0, 1/2)$ with lattice defect fractions of 77% and 23%. A similar defect was observed previously in crystals of 1918 H1N1 NA [23]. We built a composite model to represent the molecules in translated layers with occupancies of 0.8 and 0.2. In the composite model, a portion of each dimer overlaps. This portion represents approximately one-third of the dimer and does not include the active site (Supplementary Fig. S1 A). Because one dimer had a high occupancy factor (0.8), the electron density in the overlapping region was of good quality. The low-occupancy model was built accordingly, even in the absence of high-quality electron density. The RMSD value for superposition of the 780 C α atoms of the two overlapping crystallographic dimers in the composite model was 0.163 Å, which is below values typically observed for identical structures [24]. The non-protein electron density in the active site was of good quality and allowed for modeling of **6** with full occupancy in both overlapping models (Supplementary Fig. S1 B, C). Only the high-occupancy model was used for structural analysis (Fig. 3A).

2.5. Structural comparisons

As expected, **6** binds in the active site of NA (Fig. 3A). The binding mode of **6** to NA2009_{wt} was very similar to that of oseltamivir carboxylate (PDB code 3TI6, [17]). The RMSD value for superposition of the 19 corresponding atoms of **6** and **1** was 0.193 Å. Consequently, the interactions of the two inhibitors with the protein residues are almost identical. The position of the phosphonate group of **6** overlaps with the carboxylate moiety of **1**. Strong electrostatic interactions between three arginine residues and the carboxylate of **1**, which are crucial for the inhibitor's high affinity [17], are also formed by the phosphonate group of **6** (Fig. 3B). The third oxygen atom of the phosphonate moiety points toward the opening of the active site and is not engaged in any direct interactions with protein residues. It forms a water-mediated contact with the Asp151 side-chain (Fig. 3B). Result of a detailed hydrogen bond analysis is shown in Supplementary Table S1.

3. Conclusion

Emergence of pandemic influenza strains and increasing resistance to available antiviral drugs have underscored the need for new therapeutics to combat the pathogen. Recently, the phosphonate moiety was introduced into oseltamivir as an isostere of carboxylate [12]. We prepared the phosphonate-containing inhibitor tamiphosphor and its derivatives by a modified procedure reported by Gunasekera [14]. We tested the ability of these molecules to inhibit the ectodomain of NA from the pandemic virus A/California/07/2009, using the fluorogenic substrate 4-MUNANA in our enzymatic assay. We confirmed the importance of at least one acidic moiety; it is essential for effective interaction between the inhibitor and the arginine triad. The affinity of tamiphosphor for NA was comparable to that of oseltamivir carboxylate. We did not observe any improvement in binding when we substituted the amino group in oseltamivir carboxylate or tamiphosphor with a guanidino group.

The catalytic domain of pandemic NA was successfully co-crystallized with tamiphosphor. Although the crystal contained a lattice-translocation defect in which the same portion of two dimers overlapped, the structure was refined using data to resolution 1.8 Å. Tamiphosphor was bound in the active site of NA, and its interactions with the enzyme were comparable to those of oseltamivir carboxylate [17]. The position of the phosphonate of tamiphosphor overlapped with the carboxylate of oseltamivir, and both formed comparable interactions with the arginine triad. Identical binding modes of oseltamivir and tamiphosphor is consistent with their comparable inhibition constants. Our crystal structure did not confirm the more extensive hydrogen bonding interactions predicted for **6** by molecular docking experiments [12]. The only additional interaction is mediated by the third oxygen of the phosphonate of **6**, which is exposed to solvent and formed a water-mediated contact with the Asp151 side chain. Structural information on interaction of **6** with the NA active site is useful in designing second generation derivatives with high inhibitory activities.

The successful development of adaptive inhibitors requires additional biochemical techniques such as microcalorimetry for complete description of the enzyme-inhibitor interactions. To our

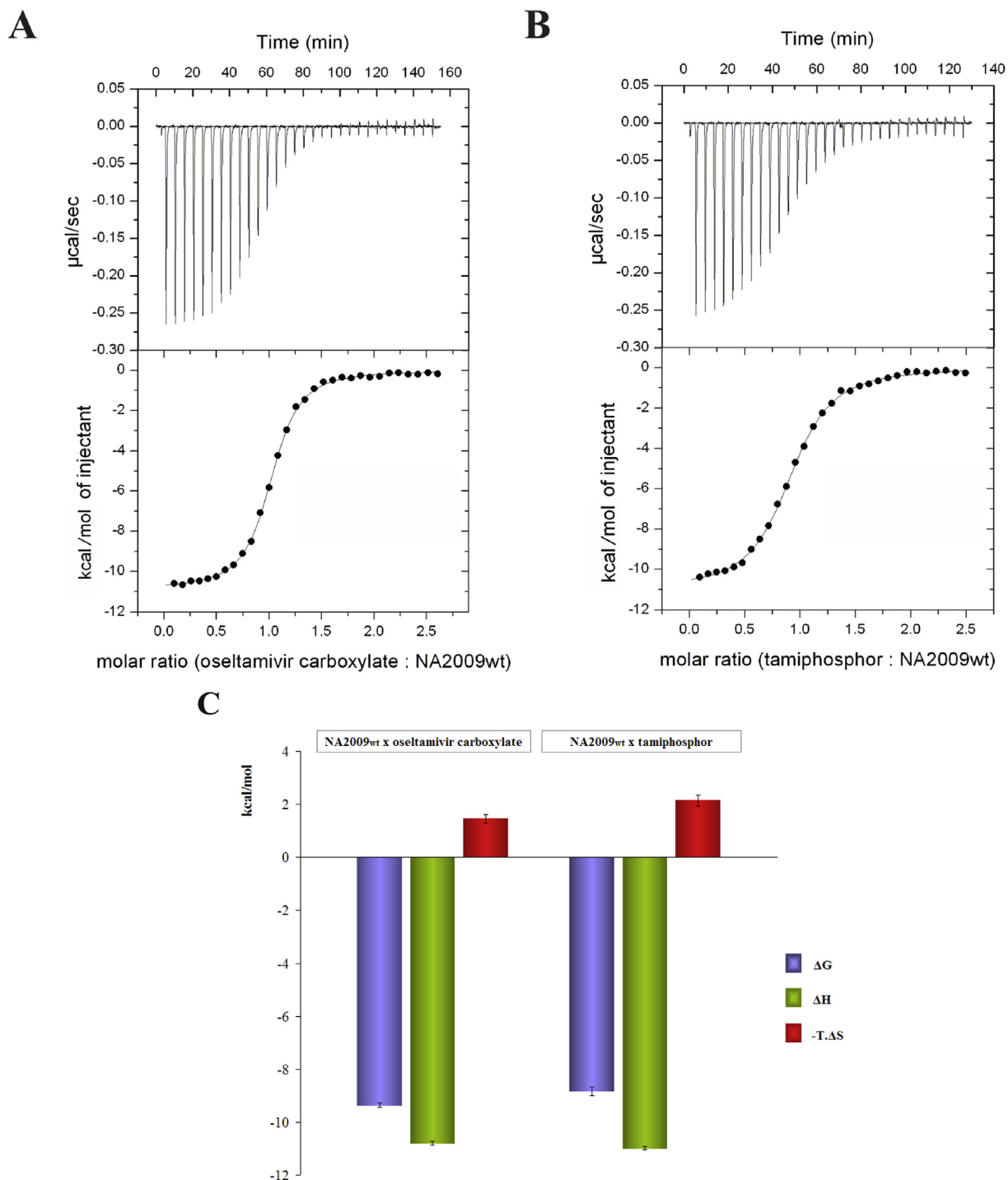


Fig. 2. Calorimetric titrations of the NA2009_{wt} catalytic domain with oseltamivir carboxylate (A) and tamiphosphor (B) performed in 50 mM MES, pH 6.15, containing 150 mM NaCl, 10 mM CaCl₂ at 25 °C. C) Graphical comparison of the thermodynamic parameters of oseltamivir carboxylate and tamiphosphor binding to the NA2009_{wt} catalytic domain.

knowledge, no calorimetric determination of binding mode has yet been published for FDA-approved NA inhibitors. We performed ITC analysis of oseltamivir carboxylate and tamiphosphor binding to the ectodomain of pandemic NA overexpressed in *Drosophila* Schneider S2 cells. Oseltamivir carboxylate was identified as an enthalpically driven NA inhibitor with a large favorable enthalpic and low unfavorable entropic contribution. Tamiphosphor bound to NA with a similar enthalpic contribution, which is in agreement

with the near-identical binding mode of both inhibitors determined by X-ray structural analysis. The entropic contribution for tamiphosphor binding was slightly less favorable (by almost 0.7 kcal/mol) as compared with oseltamivir carboxylate, which can be explained by burial of the more hydrophilic phosphonate moiety in the active site.

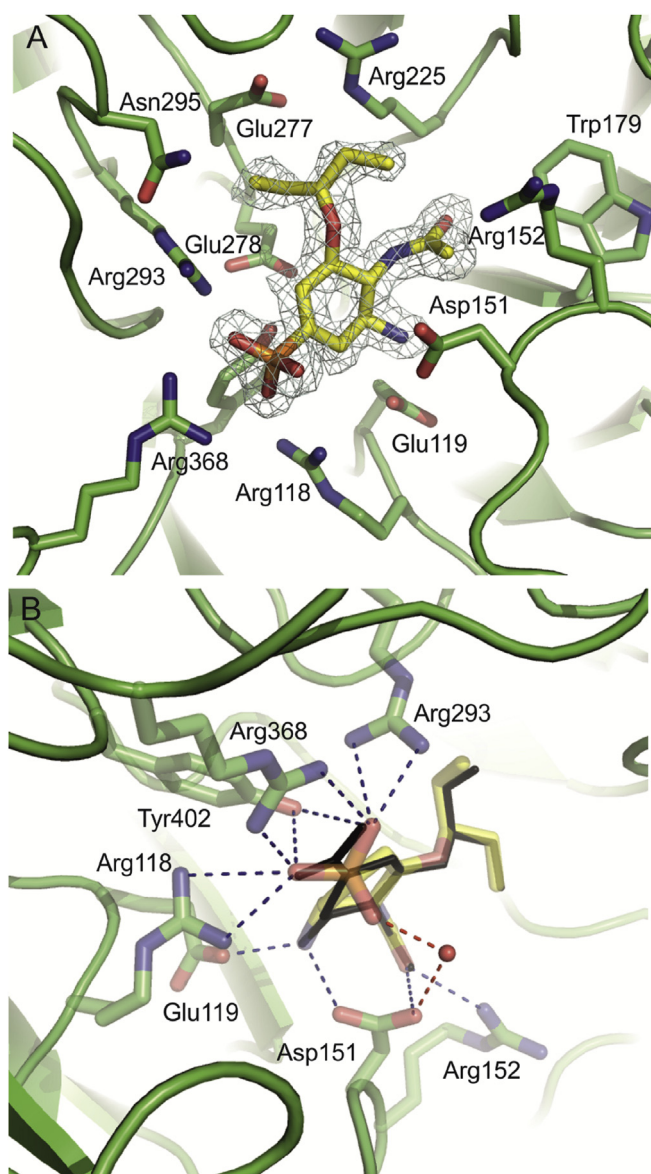


Fig. 3. Crystal structure of NA2009_{wt} in complex with tamiphosphor. A) Detail of the NA2009_{wt} active site with tamiphosphor represented by sticks with carbon atoms colored yellow. The $2F_o - F_c$ electron density map for the inhibitor contoured at 1.0σ is shown. All residues forming polar or non-polar interactions with the inhibitor are shown. B) Hydrogen bonding interactions of tamiphosphor with NA2009_{wt} and structural comparison with oseltamivir carboxylate (from PDB entry 3TI6, shown in black lines) [17]. Direct hydrogen bonds that are identical for tamiphosphor and oseltamivir carboxylate are represented by blue dash lines. The water-mediated hydrogen bond of tamiphosphor is represented by red dotted lines.

4. Experimental section

4.1. Preparation of neuraminidase inhibitors

Unless otherwise noted, all reactions were carried out under argon in oven-dried glassware. The solvents used for reactions were distilled from drying agents indicated and were transferred under argon: THF (Na/benzophenone), toluene (Na/benzophenone), MeCN (CaH₂), DCM (CaH₂). Chromatography was performed using Fluka silica gel 60 (0.040–0.063 mm) or Merck silica gel 60 RP-18 F₂₅₄ –coated aluminum sheets were used. The spots were detected both in UV and by the solution of Ce(SO₄)₂·4H₂O (1%) and H₃P(Mo₃O₁₀)₄ (2%) in 10% sulfuric acid (10%). All starting materials

were used as purchased (Sigma Aldrich, Alfa Aesar, Strem Chemicals), unless otherwise indicated. Oseltamivir phosphate was purchased from Santiago. All tested inhibitors were purified using preparative HPLC of Jasco brand (flow rate 10 mL/min; gradient 2–100% ACN in 30 min) with column Watex C18 Analytical Column, 5 μ m, length 250 mm. The final inhibitors were all at least of 95% purity. The ¹H NMR spectra were recorded on Bruker instruments at 300, 400 or 600 MHz, the ¹³C NMR spectra at were recorded at 75, 100 or 150 MHz, respectively. Tetramethylsilane or *t*-BuOH were used as an internal standards. The chemical shifts are given in δ -scale, coupling constants *J* are given in Hz. The EI mass spectra were determined at an ionizing voltage of 70 eV, the *m/z* values are given alone with their relative intensities (%). The ESI mass spectra were recorded using ZQ micromass mass spectrometer (Waters) equipped with an ESCi multimode ion source and controlled by MassLynx software. Methanol was used as solvent.

4.1.1. Oseltamivir carboxylate (**1**)

An aqueous solution of NaOH (0.5 M; 1.9 mL) was added dropwise to a stirred solution of oseltamivir phosphate (0.2 g, 0.48 mmol) in 1,4-dioxane (1.9 mL). The reaction was stirred for 24 h at room temperature. The pH was adjusted to neutral by addition of Amberlite IR 120 hydrogen form. After removal of Amberlite the filtrate was concentrated under reduced pressure and the formed residue was purified by preparative HPLC to furnish the free amine derivative **1** (0.12 g, 88% yield). ¹H NMR (400 MHz, MeOD) δ 6.64 (s, 1H), 4.11 (d, *J* = 8.5 Hz, 1H), 3.83 (dd, *J* = 11.4, 8.7 Hz, 1H), 3.40 (td, *J* = 10.8, 5.5 Hz, 1H), 3.34–3.22 (m, 1H), 3.16 (dt, *J* = 3.3, 1.6 Hz, 1H), 2.80 (dd, *J* = 17.3, 5.1 Hz, 1H), 2.38–2.18 (m, 1H), 1.91 (s, 3H), 1.47–1.28 (m, 4H), 0.75 (dt, *J* = 12.6, 7.4 Hz, 6H). ¹³C NMR (101 MHz, MeOD) δ 174.9, 169.6, 138.4, 129.8, 83.7, 76.0, 54.5, 50.5, 30.0, 27.2, 26.6, 23.4, 9.8, 9.6. HR-ESI-MS calculated for C₁₄H₂₃O₄N₂ (M–H⁺) 283.1663, found 283.1656.

4.1.2. (3*R*,4*R*,5*S*)-4-Acetamido-5-guanidino-3-(1-ethylpropoxy)-1-cyclohexene-1-carboxylic acid (**2**)

The Boc-protected intermediate **5** (0.07 g, 0.129 mmol) was stirred with trifluoroacetic acid (50% in water, 5 mL) at room temperature for 1 h. The solution was evaporated under reduced pressure and purified by preparative HPLC to furnish the guanidine derivative **2** (0.02 g, 43%). ¹H NMR (400 MHz, MeOD) δ 7.28 (d, *J* = 9.0 Hz, 1H), 6.79 (s, 1H), 4.15 (dd, *J* = 5.3, 2.1 Hz, 1H), 3.93–3.73 (m, 2H), 3.42–3.31 (m, 1H), 2.77 (dd, *J* = 17.6, 5.0 Hz, 1H), 2.37–2.20 (m, 1H), 1.94 (s, 3H), 1.48 (tdd, *J* = 12.9, 6.2, 4.5 Hz, 4H), 0.86 (dt, *J* = 12.8, 7.4 Hz, 6H). ¹³C NMR (101 MHz, MeOD) δ 174.2, 169.0, 158.6, 138.8, 129.8, 83.8, 76.1, 55.8, 51.7, 31.3, 27.2, 26.8, 22.8, 9.8, 9.7. All spectral properties matched literature values [27]. HR-ESI-MS calculated for C₁₅H₂₇O₄N₄ (M + H)⁺ 327.2027, found 327.2028.

4.1.3. Ethyl (3*R*,4*R*,5*S*)-4-acetamido-5-amino-3-(1-ethylpropoxy)-1-cyclohexene-1-carboxylate (**3**)

To a solution of oseltamivir phosphate (1.0 g, 2.43 mmol) in water (30 mL) was added a saturated solution of sodium bicarbonate (10 mL). The reaction mixture was stirred for 5 min at room temperature. The mixture was extracted with DCM/MeOH mixture (3:1; 4 \times 10 mL). The combined organic phase was washed with brine, dried over anhydrous Na₂SO₄ and concentrated under reduced pressure to furnish the free base of oseltamivir (0.75 g, 98% yield). The product was used without further purification. ¹H NMR (300 MHz, CDCl₃) δ 6.78 (t, *J* = 2.1 Hz, 1H), 6.26 (d, *J* = 8.3 Hz, 1H), 4.34–4.10 (m, 3H), 3.55 (dt, *J* = 10.3, 8.4 Hz, 1H), 3.37 (dd, *J* = 17.7,

12.0 Hz, 1H), 3.26–3.08 (m, 1H), 2.76 (dd, $J = 17.7, 5.1$ Hz, 1H), 2.26–2.08 (m, 1H), 2.04 (s, 3H), 1.58 (s, 2H), 1.55–1.44 (m, 4H), 1.29 (t, $J = 7.1$ Hz, 3H), 0.90 (td, $J = 7.4, 3.8$ Hz, 6H). ^{13}C NMR (75 MHz, CDCl_3) δ 171.1, 166.4, 137.8, 129.5, 81.7, 77.6, 77.2, 76.7, 75.0, 60.8, 58.9, 49.3, 33.7, 26.2, 25.7, 23.6, 14.2, 9.6, 9.3. HR-ESI-MS calculated for $\text{C}_{16}\text{H}_{29}\text{O}_4\text{N}_2$ ($\text{M} + \text{H}$) $^+$ 313.2122, found 313.2122.

4.1.4. Ethyl (3*R*,4*R*,5*S*)-4-acetamido-5-[[N^2,N^3 -bis(*tert*-butoxycarbonyl)guanidino]-3-(1-ethylpropoxy)-1-cyclohexene-1-carboxylate (**4**)

Mercury(II) chloride (0.11 g, 0.406 mmol) was added portionwise to a solution of oseltamivir base **3** (0.10 g, 0.320 mmol), N,N' -di(*tert*-butoxycarbonyl)thiourea (0.11 g, 0.400 mmol) and triethylamine (0.11 mL, 0.800 mmol) in DMF (15 mL) at 0 °C. The reaction mixture was stirred for 24 h at room temperature. The mixture was diluted with EtOAc (10 mL), filtered through a pad of Celite and concentrated under reduced pressure. The residue was diluted with water (30 mL) and extracted with EtOAc (3 \times 10 mL). The combined organic phase was washed with water, brine, dried over Na_2SO_4 , filtered and evaporated. The residue was purified by flash column chromatography (eluent Hexanes/EtOAc, 2:1) to afford the Boc-protected guanidine derivative **4** (0.16 g, 89%). TLC (Hexanes/EtOAc 1:1) $R_f = 0.4$. ^1H NMR (300 MHz, CDCl_3) δ 11.33 (s, 1H), 8.57 (d, $J = 8.1$ Hz, 1H), 6.76 (s, 1H), 6.16 (d, $J = 8.9$ Hz, 1H), 4.43–4.23 (m, 1H), 4.20–4.01 (m, 3H), 3.96 (d, $J = 7.7$ Hz, 1H), 3.36–3.21 (m, 1H), 2.72 (dd, $J = 17.6, 5.3$ Hz, 1H), 2.42–2.23 (m, 1H), 1.85 (s, 3H), 1.55–1.49 (m, 22H), 1.22 (dd, $J = 12.6, 5.5$ Hz, 3H), 0.82 (dt, $J = 10.3, 7.4$ Hz, 6H). ^{13}C NMR (101 MHz, CDCl_3) δ 170.3, 166.0, 163.3, 157.0, 152.7, 138.1, 128.7, 83.6, 82.8, 79.6, 76.3, 61.1, 54.5, 48.2, 30.6, 28.41, 28.2, 26.2, 25.9, 23.4, 14.3, 9.7, 9.4. HR-ESI-MS calculated for $\text{C}_{27}\text{H}_{47}\text{O}_8\text{N}_4$ ($\text{M} + \text{H}$) $^+$ 555.3388, found 555.3389.

4.1.5. (3*R*,4*R*,5*S*)-4-Acetamido-5-[[N^2,N^3 -bis(*tert*-butoxycarbonyl)guanidino]-3-(1-ethylpropoxy)-1-cyclohexene-1-carboxylic acid (**5**)

An aqueous solution of NaOH (0.5 M; 0.55 mL) was added to a solution of ester **4** (0.15 g, 0.27 mmol) in 1,4-dioxane (0.55 mL). The reaction mixture was stirred overnight at room temperature. The pH was adjusted to neutral by addition of Amberlite IR 120 hydrogen form. Amberlite was removed and the liquid phase was concentrated under reduced pressure. The residue was purified by flash column chromatography (Toluene/EtOAc/AcOH 1:1:0.5%) to afford the free acid **5** (0.07 g, 48%). TLC (Toluene/EtOAc/AcOH 1:1:0.5%) $R_f = 0.2$. ^1H NMR (300 MHz, CDCl_3) δ 8.64 (d, $J = 8.1$ Hz, 1H), 6.82 (s, 1H), 6.23 (d, $J = 8.9$ Hz, 1H), 4.39 (dd, $J = 8.3, 6.0$ Hz, 1H), 4.26–4.16 (m, 2H), 4.16–4.08 (m, 1H), 4.06–3.98 (m, 1H), 3.41–3.29 (m, 1H), 2.78 (dd, $J = 17.6, 5.3$ Hz, 1H), 2.47–2.32 (m, 1H), 1.91 (s, 3H), 1.61–1.41 (m, 22H), 1.27 (dt, $J = 10.9, 7.1$ Hz, 4H), 0.89 (dt, $J = 10.3, 7.4$ Hz, 6H). ^{13}C NMR (75 MHz, CD_3OD) δ 173.6, 169.3, 164.4, 157.7, 153.7, 138.7, 130.4, 84.6, 84.0, 80.5, 76.6, 54.6, 50.0, 31.4, 28.5, 28.2, 27.3, 26.9, 22.7, 9.9, 9.7. HR-ESI-MS calculated for $\text{C}_{25}\text{H}_{43}\text{O}_8\text{N}_4$ ($\text{M} + \text{H}$) $^+$ 527.3075, found 527.3076.

4.1.6. (3*R*,4*R*,5*S*)-4-Acetamido-5-amino-3-(1-ethylpropoxy)-1-cyclohexene-1-phosphonate (**6**)

Trimethylsilyl bromide (0.41 mL, 3.18 mmol) and 2,6-lutidine (0.44 mL, 3.81 mmol) were added to a solution of the Boc-protected phosphonic acid **13** (0.14 g, 0.318 mmol) in DCM (10 mL) and the reaction was allowed to stir for 9 h at room temperature. The solvent was evaporated and TFA (50% in water, 10 mL) was added. Then the reaction was allowed to stir for 1 h and the solvent was evaporated under reduced pressure. The residue was purified by preparative HPLC. ^1H NMR (400 MHz, D_2O) δ 6.31 (t, $J = 17.6$ Hz, 1H), 4.25 (s, 1H), 4.07 (t, $J = 10.2$ Hz, 1H), 3.62–3.47 (m, 2H), 2.95–2.74 (m, 1H), 2.52 (d, $J = 12.1$ Hz, 1H), 2.09 (s, 3H), 1.67–1.52 (m, 3H), 1.48 (dd, $J = 14.1, 7.0$ Hz, 1H), 0.88 (dt, $J = 17.1,$

7.4 Hz, 6H). ^{13}C NMR (151 MHz, D_2O , *t*-BuOH as reference) δ 175.9, 134.2, 133.5 (d, $J = 165.8$ Hz), 85.0, 76.8 (d, $J = 18.9$ Hz), 53.7, 50.6 (d, $J = 13.7$ Hz), 30.0 (d, $J = 11.2$ Hz), 26.2, 25.9, 23.0, 9.3, 9.1. All spectral properties matched literature values [28]. HR-ESI-MS calculated for $\text{C}_{13}\text{H}_{25}\text{O}_5\text{N}_2\text{NaP}$ ($\text{M} + \text{Na}$) $^+$ 343.1393, found 343.1395.

4.1.7. Ethyl (3*R*,4*R*,5*S*)-4-acetamido-5-[(*tert*-butoxycarbonyl)-amino]-3-(1-ethylpropoxy)-1-cyclohexene-1-carboxylate (**7**)

To a solution of oseltamivir free base **3** (0.38 g, 1.21 mmol) in DCM (3 mL) was added triethylamine (0.61 g, 6.08 mmol) followed by addition of di-*tert*-butyl dicarbonate (0.53 g, 2.42 mmol) and then the reaction mixture was stirred for 4 h at room temperature. The mixture was diluted with water (10 mL) and then extracted with DCM (3 \times 10 mL). The combined organic phase was washed with brine, dried over MgSO_4 and concentrated under reduced pressure. The residue was purified by flash column chromatography (eluent DCM to DCM/MeOH, 20:1) to afford the protected amine (0.49 g, 98% yield) as a white solid. ^1H NMR (300 MHz, CDCl_3) δ 6.78 (s, 1H), 5.80 (d, $J = 8.2$ Hz, 1H), 5.11 (d, $J = 9.0$ Hz, 1H), 4.20 (q, $J = 7.1$ Hz, 2H), 4.13–4.00 (m, 1H), 3.97 (s, 1H), 3.79 (dd, $J = 9.7, 5.1$ Hz, 1H), 3.52–3.28 (m, 1H), 2.74 (dd, $J = 18.1, 4.9$ Hz, 1H), 2.29 (dd, $J = 17.7, 9.6$ Hz, 1H), 1.98 (s, 3H), 1.51 (dd, $J = 5.5, 4.1$ Hz, 4H), 1.42 (s, 9H), 1.28 (t, $J = 7.1$ Hz, 3H), 0.88 (dd, $J = 13.6, 7.3$ Hz, 6H). ^{13}C NMR (75 MHz, CDCl_3) δ 170.9, 166.1, 156.4, 137.7, 129.5, 82.3, 79.8, 76.0, 61.1, 54.5, 49.2, 31.1, 28.5, 26.3, 25.8, 23.5, 14.3, 9.6, 9.4. HR-ESI-MS calculated for $\text{C}_{21}\text{H}_{37}\text{O}_6\text{N}_2$ ($\text{M} + \text{H}$) $^+$ 413.2646, found 413.2648.

4.1.8. (3*R*,4*R*,5*S*)-4-Acetamido-5-[(*tert*-butoxycarbonyl)-amino]-3-(1-ethylpropoxy)-1-cyclohexene-1-carboxylic acid (**8**)

An aqueous solution of NaOH (0.5 M; 4.35 mmol; 8.7 mL) was added dropwise to a stirred solution of the ester **7** (0.9 g, 2.18 mmol) in 1,4-dioxane (8.7 mL). The reaction mixture was stirred for 24 h at room temperature. The pH was adjusted to neutral by addition of Amberlite IR 120 hydrogen form. Amberlite was removed and the filtrate was concentrated under reduced pressure. The residue was purified by flash column chromatography (eluent DCM/MeOH gradient 10:1 to 10:3) to furnish the free acid **8** (1.28 g, 95% yield) as a white solid. ^1H NMR (300 MHz, CDCl_3) δ 6.81 (s, 1H), 6.69 (s, 1H), 5.72 (d, $J = 9.3$ Hz, 1H), 4.02 (d, $J = 6.8$ Hz, 2H), 3.75 (dd, $J = 13.1, 8.4$ Hz, 1H), 3.39–3.26 (m, 1H), 2.70 (dd, $J = 17.5, 5.0$ Hz, 1H), 2.25 (dd, $J = 17.7, 11.1$ Hz, 1H), 1.99 (s, 3H), 1.49 (dd, $J = 14.0, 6.7$ Hz, 4H), 1.41 (s, 9H), 0.86 (dd, $J = 16.5, 7.4$ Hz, 6H). ^{13}C NMR (75 MHz, CDCl_3) δ 171.5, 169.1, 156.9, 139.2, 129.2, 82.3, 79.8, 76.2, 55.2, 49.6, 31.0, 28.5, 26.3, 25.7, 23.4, 9.8, 9.2. HR-ESI-MS calculated for $\text{C}_{19}\text{H}_{33}\text{O}_6\text{N}_2$ ($\text{M} + \text{H}$) $^+$ 385.2333, found 385.2335.

4.1.9. (3*R*,4*R*,5*S*)-4-Acetamido-5-[(*tert*-butoxycarbonyl)-amino]-3-(1-ethylpropoxy)-1-Bromocyclohexene (**9**)

S-(1-Oxido-2-pyridyl)- N,N,N' -tetramethylthiuronium hexafluorophosphate (0.22 g, 0.592 mmol) was added to a solution of the acid **8** (0.21 g, 0.538 mmol), triethylamine (0.22 mL, 1.61 mmol) and 4-(dimethylamino)pyridine (0.007 g, 0.053 mmol) in dry THF (4 mL). The reaction was stirred in the dark for 40 min at room temperature. The solvent was removed by evaporation under reduced pressure. The remaining green oil was dissolved in DCM (2 mL) and bromotrichloromethane (2 mL). The formed solution was irradiated (refluxed) with a flood lamp for 90 min. The mixture was concentrated and purified by flash column chromatography (eluent Toluene/EtOAc gradient 2:1 to 1:1) to afford the vinyl bromide (0.15 g, 66% yield). TLC (Toluene/EtOAc 1:1) $R_f = 0.45$. ^1H NMR (300 MHz, CDCl_3) δ 6.07 (s, 1H), 5.52 (d, $J = 9.4$ Hz, 1H), 5.35 (d, $J = 9.0$ Hz, 1H), 4.09 (dd, $J = 9.1, 6.8$ Hz, 1H), 3.88 (dd, $J = 7.9, 5.5$ Hz, 1H), 3.83 (s, 1H), 3.39–3.25 (m, 1H), 2.68 (m, $J = 26.0, 18.0, 6.8$ Hz, 2H), 1.99 (s, 3H), 1.59 (s, 1H), 1.49 (dd, $J = 7.3, 6.0$ Hz, 3H), 1.42 (s, 9H), 0.88 (t, $J = 7.4$ Hz, 6H). HR-ESI-MS calculated for

$C_{18}H_{31}BrO_4N_2Na$ ($M + Na$)⁺ 441.1359, found 441.1360.

4.1.10. Dimethyl (3*R*,4*R*,5*S*)-4-acetamido-5-[(*tert*-butoxycarbonyl)-amino]-3-(1-ethylpropoxy)-1-cyclohexene-1-phosphonate (**10**)

To a solution of the vinyl bromide **9** (0.18 g, 0.386 mmol) in toluene (10 mL) was added tetrakis(triphenylphosphine)palladium (0.07 g, 0.057 mmol), triethylamine (0.21 mL, 1.54 mmol) and dimethyl phosphite (0.14 mL, 1.54 mmol). The reaction mixture was stirred at 80 °C for 90 min. The reaction was quenched with a saturated solution of NH_4Cl (6 mL) and later was diluted with DCM (30 mL). The organic phase was washed with a saturated solution of NH_4Cl (6 mL) and brine (2 × 5 mL), dried over $MgSO_4$ and concentrated. The residue was purified by flash column chromatography (eluent EtOAc gradient to EtOAc/MeOH 6:1) to afford the phosphonate **10** (0.16 g, 86% yield). TLC (EtOAc/MeOH 6:1) R_f = 0.42. ¹H NMR (300 MHz, $CDCl_3$) δ 6.59 (d, J = 21.8 Hz, 1H), 6.02 (d, J = 8.8 Hz, 1H), 5.17 (d, J = 9.0 Hz, 1H), 4.11–3.99 (m, 1H), 3.94 (s, 1H), 3.77 (d, J = 11.9 Hz, 1H), 3.72 (d, J = 2.4 Hz, 3H), 3.69 (d, J = 2.4 Hz, 3H), 3.39–3.27 (m, 1H), 2.67–2.49 (m, 1H), 2.28–2.11 (m, 1H), 1.97 (s, 3H), 1.56–1.44 (m, 4H), 1.40 (s, 9H), 0.86 (td, J = 7.4, 5.1 Hz, 6H). HR-ESI-MS calculated for $C_{20}H_{37}O_7NaN_2P$ ($M + Na$)⁺ 471.2231, found 471.2232.

4.1.11. Dimethyl (3*R*,4*R*,5*S*)-4-acetamido-5-[*N*2,*N*3-bis(*tert*-butoxycarbonyl)guanidino]-3-(1-ethylpropoxy)-1-cyclohexene-1-phosphonate (**11**)

The Boc-protected phosphonate **10** (0.12 g, 0.259 mmol) was treated with trifluoroacetic acid (100%, 1 mL) for 1 h and then TFA was removed by evaporation under reduced pressure. The residue was dissolved in acetonitrile (1.5 mL). Triethylamine (0.18 mL, 1.29 mmol) was added dropwise followed by addition of *N,N'*-di-Boc-1*H*-pyrazole-1-carboximidine (0.08 g, 0.259 mmol). The reaction mixture was stirred for 18 h at room temperature and then was evaporated to dryness. The residue was purified by flash column chromatography (eluent EtOAc gradient to EtOAc/MeOH 6:1) to afford the guanidine phosphonate (0.07 g, 47% yield). ¹H NMR (300 MHz, $CDCl_3$) δ 11.39 (s, 1H), 8.60 (d, J = 7.3 Hz, 1H), 6.64 (d, J = 22.5 Hz, 1H), 6.35 (d, J = 9.2 Hz, 1H), 4.41 (d, J = 8.2 Hz, 1H), 4.23–4.04 (m, 1H), 3.99 (s, 1H), 3.73 (s, 3H), 3.70 (s, 3H), 3.39–3.27 (m, 1H), 2.72–2.58 (m, 1H), 2.36–2.22 (m, 1H), 1.92 (s, 3H), 1.58–1.41 (m, 22H), 0.88 (dd, J = 16.2, 7.4 Hz, 6H). ¹³C NMR (75 MHz, $CDCl_3$) δ 170.6, 163.2, 157.0, 152.7, 143.2, 143.1, 132.2, 132.1, 126.6, 124.1, 83.7, 82.8, 79.8, 76.4, 76.1, 54.3, 52.8, 52.7, 52.6, 52.6, 48.4, 48.2, 30.9, 30.8, 28.3, 28.1, 26.0, 25.7, 23.3, 9.6, 9.3. HR-ESI-MS calculated for $C_{26}H_{48}O_9N_4P$ ($M + H$)⁺ 591.3153, found 591.3153.

4.1.12. (3*R*,4*R*,5*S*)-4-Acetamido-5-guanidino-3-(1-ethylpropoxy)-1-cyclohexene-1-phosphonate (**12**)

Neat bromotrimethylsilane (1.49 g, 9.68 mmol) was added to a solution of the phosphonate **11** (0.07 g, 0.121 mmol) in DCM (5 mL) at 0 °C and the reaction was allowed to stir for 24 h at room temperature. The solvent was evaporated under reduced pressure; the remaining residue was quenched with water (4 mL) and then the mixture was stirred for 2 h. The solution was evaporated to dryness and later was purified by preparative HPLC to afford the free guanidine **12** (0.09 g, 21% yield). ¹H NMR (400 MHz, D_2O) δ 6.31 (d, J = 19.8 Hz, 1H), 4.26 (d, J = 8.5 Hz, 1H), 4.01–3.88 (m, 1H), 3.80 (td, J = 10.4, 5.2 Hz, 1H), 3.60–3.47 (m, 1H), 2.85–2.66 (m, 1H), 2.46–2.31 (m, 1H), 2.04 (s, 3H), 1.65–1.50 (m, 3H), 1.45 (dt, J = 14.4, 7.2 Hz, 1H), 0.87 (dt, J = 19.5, 7.4 Hz, 6H). ¹³C NMR (151 MHz, D_2O , *t*-BuOH as reference) δ 175.3, 157.6, 157.5, 135.3, 135.3, 134.0, 132.8, 85.0, 77.0, 76.9, 70.5, 55.9, 51.8, 51.7, 31.5, 31.4, 30.2, 26.3, 26.0, 22.7, 22.6, 9.3, 9.2. ³¹P NMR (162 MHz, D_2O) δ 11.13. All spectral properties matched literature values [10]. HR-ESI-MS calculated for $C_{14}H_{28}O_5N_4P$ ($M + H$)⁺ 363.1792, found 363.1794.

4.1.13. Methyl (3*R*,4*R*,5*S*)-4-acetamido-5-[(*tert*-butoxycarbonyl)-amino]-3-(1-ethylpropoxy)-1-cyclohexene-1-phosphonate (**13**)

An aqueous solution of NaOH (0.5 M; 2.8 mL) was added to a stirred solution of the dimethoxyphosphonate **10** (0.31 g, 0.698 mmol) in 1,4-dioxane (2.8 mL). The reaction mixture was stirred for 18 h at room temperature. The pH was adjusted to neutral by addition of Amberlite IR 120 hydrogen form. Later Amberlite was removed and the filtrate was concentrated under reduced pressure. The residue was purified by flash column chromatography (eluent EtOAc/MeOH gradient 6:1 to 1:2) to furnish phosphonic acid **13** (0.27 g, 91% yield) as a white solid. TLC (DCM/MeOH 2:1), R_f = 0.2. ¹H NMR (600 MHz, D_2O) δ 6.32 (d, J = 19.7 Hz, 1H), 4.25 (d, J = 8.6 Hz, 1H), 3.83 (t, J = 10.0 Hz, 1H), 3.75 (s, 1H), 3.52 (d, J = 10.7 Hz, 3H), 2.45–2.43 (m, 2H), 2.24 (s, 3H), 1.57 (dd, J = 13.6, 6.7 Hz, 4H), 1.51–1.34 (m, 9H), 0.88 (dt, J = 34.7, 7.3 Hz, 6H). ¹³C NMR (151 MHz, D_2O) δ 174.2, 157.6, 137.0, 131.6, 130.5, 84.2, 80.9, 76.9, 76.7, 55.6, 51.6, 51.6, 49.3, 49.2, 31.1, 27.6, 25.6, 25.3, 22.2, 8.6, 8.5. ³¹P NMR (121 MHz, D_2O) δ 15.27. HR-ESI-MS calculated for $C_{19}H_{36}O_7N_2P$ ($M + H$)⁺ 435.2255, found 435.2256.

4.1.14. Methyl (3*R*,4*R*,5*S*)-4-acetamido-5-amino-3-(1-ethylpropoxy)-1-cyclohexene-1-phosphonate (**14**)

The phosphonic acid **13** (0.05 g, 1.14 mmol) was stirred with trifluoroacetic acid (50% in water, 4 mL) at room temperature for 1 h. The solution was evaporated under reduced pressure and later residue was purified by preparative HPLC to furnish the title compound (0.02 g, 43% yield). ¹H NMR (600 MHz, D_2O) δ 6.38 (d, J = 19.4 Hz, 1H), 4.28 (d, J = 7.5 Hz, 1H), 4.14–4.01 (m, 1H), 3.65–3.55 (m, 2H), 3.53 (d, J = 10.8 Hz, 3H), 2.82–2.72 (m, 1H), 2.49–2.40 (m, 1H), 2.09 (s, 3H), 1.60–1.45 (m, 4H), 0.90 (t, J = 7.2 Hz, 3H), 0.85 (t, J = 7.2 Hz, 3H). ¹³C NMR (151 MHz, D_2O) δ 175.8, 137.9 (d, J = 6.8 Hz), 129.7 (d, J = 174.4 Hz), 84.9, 76.5 (d, J = 19.4 Hz), 53.5, 52.5 (d, J = 5.1 Hz), 50.3 (d, J = 14.1 Hz), 29.8 (d, J = 11.0 Hz), 26.1, 25.8, 22.9, 9.2, 9.1. HR-ESI-MS calculated for $C_{14}H_{28}O_5N_2P$ ($M + H$)⁺ 335.1730, found 335.1732.

4.2. Cloning, expression and purification of recombinant NA2009_{wt}

DNA encoding the ectodomain of neuraminidase (residues 82 to 469) from the A/California/07/2009 (H1N1) influenza virus was prepared by GenScript USA Inc. (Genbank Source Sequence [CY121682](#)). This synthetic DNA was inserted into the pMT/BiP/V5-HisA vector (Invitrogen) with an N-terminal tag containing two Strep-tags, a FLAG tag and a thrombin cleavage site. This vector was used to transfect *Drosophila* Schneider S2 cells (Invitrogen). NA2009_{wt} was secreted into the culture medium, and large-scale expression of neuraminidase with an N-terminal tag followed the protocol previously described in detail [29].

The overexpressed protein was subsequently purified by one-step purification on Strep-Tactin (IBA GmbH) [30,31]. Briefly, Strep-Tactin was equilibrated in buffer W (0.1 M Tris-HCl, pH 8.0, 0.15 M NaCl), and cell culture medium with expressed neuraminidase and added biotin blocking solution BioLock (IBA GmbH) was applied. The matrix with bound tagged protein was thoroughly washed with buffer W, and NA2009_{wt} was eluted with 10 mM desthiobiotin in buffer W. The column was regenerated with buffer W containing 1 mM 2-(4-hydroxyphenylazo)benzoic acid (Sigma-Aldrich) and stored at 4 °C for later use. The purification process was monitored by SDS PAGE and Western blot using murine monoclonal anti-FLAG M2-peroxidase antibody clone M2 (Sigma-Aldrich). The N-terminal tag was removed with thrombin protease immobilized on agarose beads (Sigma-Aldrich).

4.3. Kinetic analysis of inhibitor binding to recombinant NA2009_{wt}

Enzyme kinetic parameters were determined by fluorimetric assay using the substrate 2'-(4-methylumbelliferyl)- α -D-N-acetylneuraminic acid (4-MUNANA, Sigma-Aldrich) [15]. Substrate cleavage was monitored at excitation and emission wavelengths of 365 nm and 450 nm, respectively, using an Infinite M1000 reader (TECAN). The reactions were performed for 20 min at 37 °C. The 40 μ l reaction solutions contained 17 nM NA2009_{wt} (calculated for monomer) and increasing concentrations of substrate. The reactions were stopped by addition of 40 μ l of 1 M sodium carbonate. The inhibition constants for complexes of NA2009_{wt} with prepared inhibitors were determined by measuring the reduction in the substrate hydrolysis rate caused by different inhibitor concentrations. The data were analyzed using the equation for competitive inhibition according to Williams and Morrison [32].

4.4. Isothermal titration calorimetry

The binding of oseltamivir carboxylate (**1**) or tamiphosphor (**6**) to the catalytic domain of NA2009_{wt} was monitored at 25 °C using a VP-ITC microcalorimeter (MicroCal Inc./Malvern Instruments Ltd., UK). The reactant solutions were prepared in 50 mM MES, pH 6.15, containing 150 mM NaCl and 10 mM CaCl₂. The exact concentrations of NA2009_{wt} were determined by HPLC amino acid analysis. Inhibitor concentrations were determined by elemental analyses. Typically, 9 μ l aliquots of 76–93 μ M inhibitor were injected stepwise into the sample cell containing 1.43 mL of 6.4–6.7 μ M NA2009_{wt} until saturation was achieved. To estimate whether inhibitor binding was accompanied by proton transfer, titrations in two buffers with different ionization enthalpies (MES and ACES) were performed. Experimental titrations were accompanied by a corresponding control experiment in which ligand was injected into the buffer alone. The thermodynamic parameters were determined by MicroCal software implemented in Origin 7.0 (MicroCal Inc./Malvern Instruments Ltd., UK).

4.5. Crystallization and diffraction data collection

The NA2009_{wt}-tamiphosphor complex was prepared by mixing the enzyme in buffer containing 5 mM Tris-HCl, pH 8.0, with a 3-fold molar excess of inhibitor. The complex was concentrated to 8 mg/mL by ultrafiltration using Microcon-10 filters (Millipore, Billerica, MA, USA). Crystals were grown by hanging drop vapor diffusion at 19 °C. The crystallization drops consisted of 1 μ l NA2009_{wt}-tamiphosphor complex and 1 μ l reservoir solution. The optimized reservoir solution contained 0.1 M HEPES, pH 7.75, and 5% PEG8000.

Crystals were soaked in reservoir solution supplemented with 30% ethylene glycol and cryo-cooled in liquid nitrogen. A complete dataset at 1.8 Å resolution was collected at 100 K at beamline MX14.3 of BESSY, Berlin, Germany [33]. The dataset was processed using the HKL-3000 package [34]. The crystal parameters and data collection statistics are listed in Table 1.

4.6. Structure determination

The structure was determined by difference-Fourier method using the crystal structure of 2009 pandemic H1N1 neuraminidase complexed with oseltamivir carboxylate (PDB 3TI6) as a template [17]. Lattice-translocation defect was observed with lattice translocation vector (1/2, 0, 1/2) and the lattice defect fractions calculated from the native Patterson peak ratio were 77 and 23%, respectively [23]. A composite model was built to represent the molecules in translated and untranslated layers with occupancies

Table 1
Diffraction data collection and refinement statistics.

Data collection statistics	
Space group	C222 ₁
Cell parameters (Å)	118.9, 137.1, 118.9
Wavelength (Å)	0.8944
Resolution (Å)	50.0–1.8 (1.86–1.80)
Number of unique reflections	87,032 (7,188)
Redundancy	3.9 (2.3)
Completeness (%)	97.9 (81.2)
R _{merge} ^a	10.7 (33.8)
Average I/ σ (I)	10.32 (1.94)
Wilson B (Å ²)	10.6
Refinement statistics	
Resolution range (Å)	15.8–1.8 (1.85–1.8)
No. of reflections in working set	82,656 (4,835)
No. of reflections in test set	4,346 (267)
R value (%) ^b	16.28 (21.2)
R _{free} value (%) ^c	22.49 (33.7)
RMSD bond length (Å)	0.016
RMSD angle (°)	1.475
Mean B value (Å ²)	6.2
Number of protein atoms ^d	6,882/6,749
Number of ligand atoms ^d	42/42
Number of water molecules ^d	747/695
Ramachandran plot statistics ^e	
Residues in favored regions (%)	83.1
Residues in allowed regions (%)	16.9
PDB accession code	5D03

The data in parentheses refer to the highest-resolution shell.

^a $R_{\text{merge}} = \frac{\sum_{\text{hkl}} \sum_i |I_i(\text{hkl}) - \langle I(\text{hkl}) \rangle|}{\sum_{\text{hkl}} \sum_i I_i(\text{hkl})}$, where $I_i(\text{hkl})$ is the individual intensity of the i th observation of reflection hkl and $\langle I(\text{hkl}) \rangle$ is the average intensity of reflection hkl with summation over all data.

^b $R = \frac{\sum |F_o| - |F_c|}{\sum |F_o|}$, where F_o and F_c are the observed and calculated structure factors, respectively.

^c R_{free} is equivalent to R but is calculated for 5% of the reflections chosen at random and omitted from the refinement process [25].

^d Values for two alternative models are given.

^e As determined by Molprobtity server [26].

of 0.8 and 0.2, respectively. Model refinement was performed using the program REFMAC 5.7.0032 [35] from the CCP4 package [36] in combination with manual adjustments in Coot software [37]. Tamiphosphor was modeled after complete refinement of the protein chains and solvent model. Sugars attached to following residues were modelled: Asn 88 (chain B) and Asn146 (chain A and B). Glycosylation in position Asn 235 and Asn 386 was not modelled as the quality of the electron density maps did not allow for unambiguous tracing of sugar moieties. The Molprobtity server [26] was used for evaluation of the final model quality. The final refinement statistics are summarized in Table 1. The structures were analyzed using the programs Lsqkab (superpose) [38], Baverage and Contact from the CCP4 package [36]. Atomic coordinates and structure factors were deposited in the PDB under accession code 5D03.

Acknowledgements

The authors wish to thank Jana Starková and Iva Flaisigová for technical assistance, Radko Souček for expert amino acid analyses and Hillary Hoffman for proofreading of the manuscript. This work was supported by the Grant Agency of the Czech Republic (grant 13-19561S), in part by projects LO1302 and LO1304 from the Ministry of Education of the Czech Republic, and by research projects RVO 61388963 and RVO 68378050 from the Academy of Sciences of the Czech Republic.

Appendix A. Supplementary data

Supplementary data related to this article can be found at <http://dx.doi.org/10.1016/j.ejmech.2016.05.016>.

References

- [1] J.K. Taubenberger, D.M. Morens, 1918 Influenza: the mother of all pandemics, *Emerg. Infect. Dis.* 12 (2006) 15–22.
- [2] P. Doshi, The elusive definition of pandemic influenza, *Bull. World Health Organ.* 89 (2011) 532–538.
- [3] D. Gatherer, The 2009 H1N1 influenza outbreak in its historical context, *J. Clin. Virol.* 45 (2009) 174–178.
- [4] J. Zhou, D. Wang, R. Gao, B. Zhao, J. Song, X. Qi, Y. Zhang, Y. Shi, L. Yang, W. Zhu, T. Bai, K. Qin, Y. Lan, S. Zou, J. Guo, J. Dong, L. Dong, H. Wei, X. Li, J. Lu, L. Liu, X. Zhao, W. Huang, L. Wen, H. Bo, L. Xin, Y. Chen, C. Xu, Y. Pei, Y. Yang, X. Zhang, S. Wang, Z. Feng, J. Han, W. Yang, G.F. Gao, G. Wu, D. Li, Y. Wang, Y. Shu, Biological features of novel avian influenza A (H7N9) virus, *Nature* 499 (2013) 500–503.
- [5] M. von Itzstein, The war against influenza: discovery and development of sialidase inhibitors, *Nat. Rev. Drug Discov.* 6 (2007) 967–974.
- [6] R.J. Jackson, K.L. Cooper, P. Tappenden, A. Rees, E.L. Simpson, R.C. Read, K.G. Nicholson, Oseltamivir, zanamivir and amantadine in the prevention of influenza: a systematic review, *J. Infect.* 62 (2011) 14–25.
- [7] A. Loregian, B. Mercorelli, G. Nannetti, C. Compagnin, G. Palu, Antiviral strategies against influenza virus: towards new therapeutic approaches, *Cell Mol. Life Sci.* 71 (2014) 3659–3683.
- [8] H. Ohtaka, E. Freire, Adaptive inhibitors of the HIV-1 protease, *Prog. Biophys. Mol. Biol.* 88 (2005) 193–208.
- [9] X. Zhu, R. McBride, C.M. Nycholat, W. Yu, J.C. Paulson, I.A. Wilson, Influenza virus neuraminidases with reduced enzymatic activity that avidly bind sialic acid receptors, *J. Virol.* 86 (2012) 13371–13383.
- [10] T.J. Cheng, S. Weinheimer, E.B. Tarbet, J.T. Jan, Y.S. Cheng, J.J. Shie, C.L. Chen, C.A. Chen, W.C. Hsieh, P.W. Huang, W.H. Lin, S.Y. Wang, J.M. Fang, O.Y. Hu, C.H. Wong, Development of oseltamivir phosphonate congeners as anti-influenza agents, *J. Med. Chem.* 55 (2012) 8657–8670.
- [11] R.J. Russell, L.F. Haire, D.J. Stevens, P.J. Collins, Y.P. Lin, G.M. Blackburn, A.J. Hay, S.J. Gamblin, J.J. Skehel, The structure of H5N1 avian influenza neuraminidase suggests new opportunities for drug design, *Nature* 443 (2006) 45–49.
- [12] J.J. Shie, J.M. Fang, S.Y. Wang, K.C. Tsai, Y.S. Cheng, A.S. Yang, S.C. Hsiao, C.Y. Su, C.H. Wong, Synthesis of tamiflu and its phosphonate congeners possessing potent anti-influenza activity, *J. Am. Chem. Soc.* 129 (2007) 11892–11893.
- [13] C.L. Chen, T.C. Lin, S.Y. Wang, J.J. Shie, K.C. Tsai, Y.S. Cheng, J.T. Jan, C.J. Lin, J.M. Fang, C.H. Wong, Tamiphosphor monoesters as effective anti-influenza agents, *Eur. J. Med. Chem.* 81 (2014) 106–118.
- [14] D.S. Gunasekera, Formal synthesis of tamiflu: conversion of tamiflu into tamiphosphor, *Synlett* (2012) 573–576.
- [15] M. Potier, L. Mameli, M. Belisle, L. Dallaire, S.B. Melancon, Fluorometric assay of neuraminidase with a sodium (4-methylumbelliferyl- α -D-N-acylneuraminyl) substrate, *Anal. Biochem.* 94 (1979) 287–296.
- [16] R. Xu, X. Zhu, R. McBride, C.M. Nycholat, W. Yu, J.C. Paulson, I.A. Wilson, Functional balance of the hemagglutinin and neuraminidase activities accompanies the emergence of the 2009 H1N1 influenza pandemic, *J. Virol.* 86 (2012) 9221–9232.
- [17] C.J. Vavricka, Q. Li, Y. Wu, J. Qi, M. Wang, Y. Liu, F. Gao, J. Liu, E. Feng, J. He, J. Wang, H. Liu, H. Jiang, G.F. Gao, Structural and functional analysis of laninamivir and its octanoate prodrug reveals group specific mechanisms for influenza NA inhibition, *PLoS Pathog.* 7 (2011) e1002249.
- [18] E. Freire, Do enthalpy and entropy distinguish first in class from best in class? *Drug Discov. Today.* 13 (2008) 869–874.
- [19] M. Kozisek, J. Bray, P. Rezacova, K. Saskova, J. Brynda, J. Pokorna, F. Mammano, L. Rulisek, J. Konvalinka, Molecular analysis of the HIV-1 resistance development: enzymatic activities, crystal structures, and thermodynamics of nelfinavir-resistant HIV protease mutants, *J. Mol. Biol.* 374 (2007) 1005–1016.
- [20] M. Kozisek, M. Lepsik, K. Grantz Saskova, J. Brynda, J. Konvalinka, P. Rezacova, Thermodynamic and structural analysis of HIV protease resistance to darunavir – analysis of heavily mutated patient-derived HIV-1 proteases, *FEBS J.* 281 (2014) 1834–1847.
- [21] M.N. Nalam, A. Ali, M.D. Altman, G.S. Reddy, S. Chellappan, V. Kairys, A. Ozen, H. Cao, M.K. Gilson, B. Tidor, T.M. Rana, C.A. Schiffer, Evaluating the substrate-envelope hypothesis: structural analysis of novel HIV-1 protease inhibitors designed to be robust against drug resistance, *J. Virol.* 84 (2010) 5368–5378.
- [22] A.J. Ruben, Y. Kiso, E. Freire, Overcoming roadblocks in lead optimization: a thermodynamic perspective, *Chem. Biol. Drug Des.* 67 (2006) 2–4.
- [23] X. Zhu, X. Xu, I.A. Wilson, Structure determination of the 1918 H1N1 neuraminidase from a crystal with lattice-translocation defects, *Acta Crystallogr. D Biol. Crystallogr.* D64 (2008) 843–850.
- [24] M.J. Betts, M.J. Sternberg, An analysis of conformational changes on protein-protein association: implications for predictive docking, *Protein Eng.* 12 (1999) 271–283.
- [25] A.T. Brunger, Free R value: a novel statistical quantity for assessing the accuracy of crystal structures, *Nature* 355 (1992) 472–475.
- [26] S.C. Lovell, I.W. Davis, W.B. Arendall 3rd, P.I. de Bakker, J.M. Word, M.G. Prisant, J.S. Richardson, D.C. Richardson, Structure validation by Calpha geometry: phi, psi and Cbeta deviation, *Proteins* 50 (2003) 437–450.
- [27] C.A. Mooney, S.A. Johnson, P. t Hart, L. Quarles van Ufford, C.A. de Haan, E.E. Moret, N.I. Martin, Oseltamivir analogues bearing N-substituted guanidines as potent neuraminidase inhibitors, *J. Med. Chem.* 57 (2014) 3154–3160.
- [28] B. Carbain, P.J. Collins, L. Callum, S.R. Martin, A.J. Hay, J. McCauley, H. Streicher, Efficient synthesis of highly active phospho-isosteres of the influenza neuraminidase inhibitor oseltamivir, *ChemMedChem.* 4 (2009) 335–337.
- [29] C. Barinka, M. Rinnova, P. Sacha, C. Rojas, P. Majer, B.S. Slusher, J. Konvalinka, Substrate specificity, inhibition and enzymological analysis of recombinant human glutamate carboxypeptidase II, *J. Neurochem.* 80 (2002) 477–487.
- [30] T.G. Schmidt, L. Batz, L. Bonet, U. Carl, G. Holzapfel, K. Kiem, K. Matulewicz, D. Niermeier, I. Schuchardt, K. Stanar, Development of the Twin-Strep-tag(R) and its application for purification of recombinant proteins from cell culture supernatants, *Protein Expr. Purif.* 92 (2013) 54–61.
- [31] T.G. Schmidt, A. Skerra, The Strep-tag system for one-step purification and high-affinity detection or capturing of proteins, *Nat. Protoc.* 2 (2007) 1528–1535.
- [32] J.W. Williams, J.F. Morrison, The kinetics of reversible tight-binding inhibition, *Methods Enzymol.* 63 (1979) 437–467.
- [33] U. Mueller, N. Darowski, M.R. Fuchs, R. Forster, M. Hellmig, K.S. Paithankar, S. Puhlinger, M. Steffien, G. Zocher, M.S. Weiss, Facilities for macromolecular crystallography at the helmholtz-zentrum Berlin, *J. Synchrotron Radiat.* 19 (2012) 442–449.
- [34] W. Minor, M. Cymborowski, Z. Otwinowski, M. Chruszcz, HKL-3000: the integration of data reduction and structure solution—from diffraction images to an initial model in minutes, *Acta Crystallogr. D Biol. Crystallogr.* 62 (2006) 859–866.
- [35] G.N. Murshudov, A.A. Vagin, E.J. Dodson, Refinement of macromolecular structures by the maximum-likelihood method, *Acta Crystallogr. D Biol. Crystallogr.* 53 (1997) 240–255.
- [36] Collaborative Computational Project, N, The CCP4 suite: programs for protein crystallography, *Acta Crystallogr. D Biol. Crystallogr.* 50 (1994) 760–763.
- [37] P. Emsley, K. Cowtan, Coot: model-building tools for molecular graphics, *Acta Crystallogr. D Biol. Crystallogr.* 60 (2004) 2126–2132.
- [38] E. Krissinel, K. Henrick, Secondary-structure matching (SSM), a new tool for fast protein structure alignment in three dimensions, *Acta Crystallogr. Sect. D Biological Crystallogr.* 60 (2004) 2256–2268.